Geophysical Research Letters

RESEARCH LETTER
10.1029/2020GL091198

D. Lohse and O. Shishkina contributed equally to this work.

Key Points:

- A unifying theory on heat and momentum transport is offered for turbulent purely internally heated convection
- The results of unifying theory are consistent with our direct numerical simulations

Correspondence to:
D. Lohse and O. Shishkina,
d.lohse@utwente.nl;
Olga.Shishkina@ds.mpg.de

Citation:
Wang, Q., Lohse, D., & Shishkina, O. (2021). Scaling in internally heated convection: A unifying theory. *Geophysical Research Letters*, *48*, e2020GL091198. https://doi.org/10.1029/2020GL091198

Received 12 OCT 2020
Accepted 30 NOV 2020

Scaling in Internally Heated Convection: A Unifying Theory

Qi Wang[1,2], Detlef Lohse[1,3], and Olga Shishkina[3]

[1]Physics of Fluids Group and Max Planck Center for Complex Fluid Dynamics, MESA+ Institute and J. M. Burgers Centre for Fluid Dynamics, University of Twente, Enschede, The Netherlands, [2]Department of Modern Mechanics, University of Science and Technology of China, Hefei, China, [3]Max Planck Institute for Dynamics and Self-Organization, Göttingen, Germany

Abstract We offer a unifying theory for turbulent, purely internally heated convection, generalizing the unifying theories of Grossmann and Lohse (2000, https://doi.org/10.1017/S0022112099007545; 2001, https://doi.org/10.1103/PhysRevLett.86.3316) for Rayleigh-Bénard turbulence and of Shishkina et al. (2016, https://doi.org/10.1002/2015GL067003) for turbulent horizontal convection, which are both based on the splitting of the kinetic and thermal dissipation rates in respective boundary and bulk contributions. We obtain the mean temperature of the system and the Reynolds number (which are the response parameters) as function of the control parameters, namely the internal thermal driving strength (called, when nondimensionalized, the Rayleigh-Roberts number) and the Prandtl number. The results of the theory are consistent with our direct numerical simulations of the Boussinesq equations.

Plain Language Summary Internally heated convection (IHC), that is, convective fluid motions driven by the internal heat generation, is an omnipresent phenomenon in many geo- and astrophysical convective flows. An important question for IHC is how the mean temperature and the global flow strength depend on the internal heating rate and the operating fluid. In this work, we offer a unifying theory to address this question. The results of the theory agree well with our direct numerical simulations.

1. Introduction

Thermally driven turbulence is omnipresent in nature and technology. The thermal driving can be thanks to the temperature boundary conditions such as in Rayleigh-Bénard convection (RBC)—a flow in a container heated from below and cooled from above (Ahlers et al., 2009; Chilla & Schumacher, 2012; Lohse & Xia, 2010)—or in horizontal convection (HC) (Hughes & Griffiths, 2008; Shishkina & Wagner, 2016; Shishkina et al., 2016) or vertical convection (Ng et al., 2015, 2017, 2018; Shishkina, 2016), where parts of the top, bottom, or sidewalls of the container are set at different temperatures. However, the thermal driving can also be thanks to internal heating, where the temperature field is driven by some forcing in the bulk. In many cases in nature, both ways of driving play a role at the same time. For example, this holds for the Earth's mantle due to the driving through the hot inner core of the Earth and an additional driving due to the decay of radioactive materials, producing heat (Bercovici et al., 1989; Bunge et al., 1996; Houseman, 1988; Lay et al., 2008; Mallard et al., 2016; Moore & Webb, 2013; Schubert et al., 2001; Tackley et al., 1993). Thus, in the Earth's mantle, about 10%–20% of the heat is transferred from the core, while the rest occurs due to the internal heating (Schubert et al., 2001). The internal heating dominates also in the atmosphere of Venus (Tritton, 1975; Tritton and Zarraga, 1967), which is heated up due to the absorption of sun light. One more example is the formation of Pluto's polygonal terrain, which is caused not only by convection of Rayleigh-Bénard type (McKinnon et al., 2016; Trowbridge et al., 2016), but also by internally heated convection (IHC) (Vilella & Deschamps, 2017). And, of course, IHC is relevant in many engineering applications, for example, liquid-metal batteries (Kim et al., 2013; Xiang & Zikanov, 2017).

To obtain a theoretical understanding of thermally driven turbulence including the cases of mixed thermal driving, it is mandatory to first understand the pure and well-defined cases, namely on the one hand turbulent RBC (exclusively driven by the heated and cooled plates), and on the other hand turbulent purely IHC (exclusively driven by thermal forcing of the temperature field in the bulk), see Roberts (1967), Goluskin

and Spiegel (2012), Goluskin and van der Poel (2016), Goluskin (2016), and Vilella et al. (2018). For the former case, Grossmann and Lohse (GL) have developed a unifying theory (Grossmann & Lohse, 2000, 2001, 2002, 2004; Stevens et al., 2013), with which the heat transfer and the degree of turbulence can quantitatively be described as function of the control parameters, in excellent agreement with the experimental and numerical data over a range of more than 7 orders of magnitude in the control parameters *Ra* and *Pr*. Later this theory was also extended to HC (Shishkina et al., 2016) and double diffusive convection (Y. Yang et al., 2018). GL arguments were also applied to IHC, to estimate the bulk temperature for small and moderate *Pr* (Goluskin & Spiegel, 2012). A complete theory, however, does not yet exist for purely IHC.

The objective of the present work is to apply the reasoning of GL's theory to the case of purely IHC and to develop a unifying theory for this case. In addition, we perform direct numerical simulations (DNS) of turbulent purely IHC over a large range of control parameters and compare the DNS results with the theoretical predictions. The DNS are conducted in two dimensions (2-D), as (i) the theory is based on Prandtl's equations, which are also 2-D in spirit, as (ii) 2-D and 3-D thermally driven turbulence show very close analogies with respect to the integral quantities, in particular for large Prandtl numbers $Pr \geq 1$ (van der Poel et al., 2013), and as (iii) otherwise, due to unavoidable limitations in available CPU time, we could explore only a much smaller portion of the parameter space.

2. Control and Response Parameters and Governing Equations

In RBC, next to the geometric aspect ratio Γ of the sample (the ratio between lateral and vertical extensions), the control parameters of the system are the temperature difference between top and bottom wall (in dimensionless form, the Rayleigh number) and the ratio between kinematic viscosity ν and thermal diffusivity κ, namely the Prandtl number $Pr = \nu/\kappa$. The response of the system consists of the heat flux from bottom to top (in dimensionless form, the Nusselt number *Nu*) and the degree of turbulence (in dimensionless form, the Reynolds number *Re*). In IHC, instead of the Rayleigh number, the dimensionless driving strength *Rr* of the temperature field takes the role of the second control parameter, next to *Pr*. It is often called Rayleigh-Roberts number (and that is why we use the abbreviation *Rr*) and will be defined below. The main response parameter, next to *Re*, is the mean temperature which the bulk achieves thanks to the internal driving. This is related to the heat fluxes into the top and bottom plates; note that they are different from each other. So the objective of this paper is to explain how the mean temperature and the Reynolds number in turbulent IHC depend on *Rr* and *Pr*, for large enough aspect ratio Γ of the sample.

The flow in IHC is confined between two parallel plates with distance L, with the gravitational acceleration $\mathrm{g} \equiv -g\mathrm{e}_z$ acting orthogonally to these plates. The underlying dynamical equations within the Boussinesq approximation are the compressibility condition $\partial_i u_i = 0$, and

$$\partial_t u_i + u_j \partial_j u_i = -\partial_i p + \nu \partial_j^2 u_i + \beta g \delta_{iz} \theta, \tag{1}$$

$$\partial_t \theta + u_j \partial_j \theta = \kappa \partial_j^2 \theta + \Omega, \tag{2}$$

for the velocity field $\boldsymbol{u}(\boldsymbol{x}, t)$, the kinematic pressure field $p(\boldsymbol{x}, t)$, and the reduced temperature field $\theta(\boldsymbol{x}, t) \equiv T(\boldsymbol{x}, t) - T_{\mathrm{plate}}$. Here T_{plate} is the temperature of both top and bottom plates, β is the thermal expansion coefficient, δ_{ij} the Kronecker delta and Ω the constant bulk driving of the temperature field, which in nondimensional form is called Rayleigh-Roberts number

$$Rr = \beta g L^5 \Omega / (\kappa^2 \nu). \tag{3}$$

Equations 1 and 2 are supplemented by the boundary conditions (BCs) $u_i = 0$ and $\theta = 0$ at both plates. Periodic BCs are used in the horizontal direction.

The main responses of the system can be expressed in terms of the mean temperature $\Delta \equiv \langle \theta(\boldsymbol{x},t) \rangle_V$ achieved in the system, where the average $\langle \cdot \rangle_V$ is over volume and time. The nondimensional form of this response parameter is

$$\tilde{\Delta} \equiv \kappa \Delta / (\Omega L^2). \tag{4}$$

The other main nondimensional response parameter is the Reynolds number $Re = UL/\nu$, with $U \equiv \sqrt{\boldsymbol{u}^2}_V$. There are different definitions of the Reynolds number (Ahlers et al., 2009), while these different *Re* usually have similar power-law dependence on *Ra*. In DNS, one usually looks at the *Re* based on the global volume averaged root-mean-square velocity, as this *Re* reflects the flow strength of the whole flow field (Shishkina & Horn, 2016; Stevens et al., 2018; van der Poel et al., 2013; Wang et al., 2020a, 2020b; R. Yang et al., 2020).

Obviously, due to the internal heating, the heat flux

$$Q(z) \equiv \langle u_z\theta\rangle - \kappa\langle\partial_z\theta\rangle \tag{5}$$

(or in dimensionless form $\tilde{Q}(z) \equiv Q(z) / (\Omega L)$) in the system is not constant as in RBC, but depends on the height z. Here, $\langle\cdot\rangle$ means average in time and in a plane of constant z. However, a simple time and plane average of Equation 2 yields that the quantity

$$\tilde{Q}_0 \equiv z / L - \tilde{Q}(z) \tag{6}$$

is constant for all z and equals

$$\tilde{Q}_0 = -\tilde{Q}(z=0) = \frac{\kappa}{\Omega L}\langle\partial_z\theta\rangle\,|_{z=0} \geq 0. \tag{7}$$

$\tilde{Q}_0$ is thus a further dimensionless response parameter of the system. Equation 7 implies that the dimensionless heat flux $\tilde{Q}$ is nonpositive at $z = 0$. Applying Equation 6 at $z = L$ gives the dimensionless flux at $z = L$,

$$\tilde{Q}(z=L) = -\frac{\kappa}{\Omega L}\langle\partial_z\theta\rangle\,|_{z=L} = 1 - \tilde{Q}_0 \geq 0, \tag{8}$$

Relations 7 and 8 immediately show that $0 \leq \tilde{Q}_0 \leq 1$.

3. Application of Grossmann and Lohse's Unifying Theory

As it is well known (Ahlers et al., 2009; Shraiman & Siggia, 1990), in RBC exact relations between the time and volume averaged thermal and kinetic dissipation rates, $\epsilon_\theta \equiv \kappa\langle(\partial_i\theta(\mathrm{x},t))^2\rangle_V$ and $\epsilon_u \equiv \nu\langle(\partial_i u_j(\mathrm{x},t))^2\rangle_V$, and the dimensionless control and response parameters *Nu*, *Ra*, and *Pr* can be obtained from multiplying the thermal advection equation with $\theta(\boldsymbol{x}, t)$ and the Navier-Stokes equation with $u_i(\boldsymbol{x}, t)$ and subsequent Gauss integration and time and space averaging. Here, we apply the same procedure to Equations 2 and 1 and obtain

$$\epsilon_\theta = \Omega\Delta = \frac{L^2}{\kappa}\Omega^2\tilde{\Delta} = \frac{\kappa\Delta^2}{L^2}\tilde{\Delta}^{-1}, \tag{9}$$

$$\epsilon_u = \frac{\nu^3}{L^4}RrPr^{-2}\left(\frac{1}{2} - \tilde{Q}_0\right). \tag{10}$$

As $\epsilon_u \geq 0$ is nonnegative by definition, we can now further restrain the magnitude of the dimensionless heat flux through the bottom plate: $0 \leq \tilde{Q}_0 \leq 1/2$. Just as the corresponding relations in RBC, also here, Equations 9 and 10 relate the averaged thermal and kinetic dissipation rates with the dimensionless control (*Rr*, *Pr*) and response ($\tilde{\Delta}$, $\tilde{Q}_0$) parameters.

The key idea of the GL theory (Grossmann & Lohse, 2000, 2001) is to split the kinetic and thermal dissipation rates into contributions from the corresponding boundary layers (BLs) and bulks,

$$\epsilon_u = \epsilon_{u,\mathrm{BL}} + \epsilon_{u,\mathrm{bulk}}, \quad \epsilon_\theta = \epsilon_{\theta,\mathrm{BL}} + \epsilon_{\theta,\mathrm{bulk}},$$

and to apply the respective scaling relations for those (i.e., for $\epsilon_{u,\mathrm{BL}}$, $\epsilon_{u,\mathrm{bulk}}$, $\epsilon_{\theta,\mathrm{BL}}$, and $\epsilon_{\theta,\mathrm{bulk}}$), based on BL theory and Kolmogorov's theory for fully developed turbulence in the bulk. The introduced scaling regimes I, II, III, and IV correspond to BL–BL, bulk–BL, BL–bulk, and bulk–bulk dominance in ϵ_u and ϵ_θ, respectively. Here, one should also take into account mean thicknesses of the thermal BLs (λ_θ) and viscous BLs (λ_u).

The cases $\lambda_\theta < \lambda_u$ (large Pr) and $\lambda_\theta > \lambda_u$ (small Pr) correspond to different scaling regimes, and therefore we assign the subscripts u and ℓ to regimes I, II, III and IV, which indicate the $u$pper-Pr and ℓower-Pr cases, respectively. Equating ϵ_u and ϵ_θ to their estimated either bulk or BL contributions and employing the classical Prandtl scaling relations for the BL thicknesses λ_θ and λ_u (Schlichting, 1979), one in principle obtains eight theoretically possible scaling regimes. The fractions of the phase space occupied by regimes II_u and III_ℓ are rather small, because, for example, in II_u, it is expected that $\lambda_\theta \geq \lambda_u$ due to the BL-dominance in ϵ_θ, but on the other hand, $\lambda_\theta \leq \lambda_u$ should hold due to the large Pr. By similar arguments, regime III_ℓ is also small.

The mean thicknesses of the BLs are estimated as follows: $\lambda_u \sim L / \sqrt{\mathrm{Re}}$, as in RBC (Ching et al., 2019; Grossmann & Lohse, 2000, 2001; Shishkina et al., 2015), and $\lambda_\theta \equiv 2 / (\lambda_{\theta,\mathrm{top}}^{-1} + \lambda_{\theta,\mathrm{bottom}}^{-1})$. Approximating $\partial_z \theta$ at $z = 0$ and $z = H$ with the ratio of Δ and the top and bottom thermal BL thicknesses, $\lambda_{\theta,\,\mathrm{top}}$ and $\lambda_{\theta,\,\mathrm{bottom}}$, from Equations 4, 7, and 8 we obtain $\lambda_\theta \sim L\tilde{\Delta}$.

The value of $\epsilon_{u,\mathrm{bulk}}$ is estimated as

$$\epsilon_{u,\mathrm{bulk}} \sim U \frac{U^2}{L} \frac{L - \lambda_u}{L} \approx \frac{U^3}{L} = \frac{\nu^3}{L^4} Re^3,$$

which is relevant in the ϵ_u-bulk dominating regimes II_ℓ, IV_ℓ, and IV_u, while the value of $\epsilon_{\theta,\mathrm{bulk}}$ is estimated as

$$\epsilon_{\theta,\mathrm{bulk}} \sim U \frac{\Delta^2}{L} \frac{L - \lambda_\theta}{L} \approx \frac{U\Delta^2}{L} = \frac{\kappa\Delta^2}{L^2} Pr\,Re,$$

which is relevant in the ϵ_θ-bulk dominating regime IV_ℓ. For large Pr (regimes III_u and IV_u), the thermal BL is embedded into the kinetic one and therefore in Equation 10, the magnitude of the velocity of the flow, which carries the temperature in the bulk, is reduced from U to $(\lambda_\theta/\lambda_u)U$, leading to

$$\epsilon_{\theta,\mathrm{bulk}} \sim \frac{\lambda_\theta}{\lambda_u} \frac{U\Delta^2}{L} \frac{L - \lambda_\theta}{L} \approx \frac{\kappa\Delta^2}{L^2} Pr\,Re^{3/2}\tilde{\Delta}. \tag{11}$$

The kinetic dissipation rate in the BL is $\sim \nu(U / \lambda_u)^2$. Hence,

$$\epsilon_{u,\mathrm{BL}} \sim \nu \frac{U^2}{\lambda_u^2} \frac{\lambda_u}{L} = \frac{\nu^3}{L^4} Re^{5/2}, \tag{12}$$

which is relevant in the ϵ_u-BL dominating regimes I_ℓ, I_u, and III_u. As in Grossmann and Lohse (2000, 2001), the factor λ_u/L accounts for the volume fraction of the kinetic BL. With increasing Pr, λ_u saturates to $\sim L$, so this factor becomes one (just as argued in Grossmann and Lohse [2001]), which yields

$$\epsilon_{u,\mathrm{BL}} \sim \nu \frac{U^2}{\lambda_u^2} = \frac{\nu^3}{L^4} Re^2. \tag{13}$$

For small Ra or very large Pr, this leads to special regimes $\mathrm{I}_\infty^<$ and III_∞ on top of, respectively, I_u and III_u. In III_∞, also $\epsilon_{\theta,\mathrm{bulk}}$ scales differently to (11), namely as

$$\epsilon_{\theta,\mathrm{bulk}} \sim \frac{\lambda_\theta}{L} \frac{U\Delta^2}{L} \frac{L - \lambda_\theta}{L} \approx \frac{\kappa\Delta^2}{L^2} Pr\,Re\tilde{\Delta}.$$

The thermal dissipation rate in the BL scales as $\sim \kappa(\Delta / \lambda_\theta)^2$, which is relevant in the ϵ_θ-BL dominating regimes I_ℓ, I_u, $\mathrm{I}_\infty^<$ and II_ℓ. This (again with the volume fraction factor) leads to

$$\epsilon_{\theta,\mathrm{BL}} \sim \kappa \frac{\Delta^2}{\lambda_\theta^2} \frac{\lambda_\theta}{L} = \kappa \frac{\Delta^2}{L^2} \frac{\lambda_u}{\lambda_\theta} Re^{1/2}. \tag{14}$$

In the limiting regimes I_ℓ, II_ℓ and $\mathrm{I}_\infty^<$, it holds $\lambda_u/\lambda_\theta \sim Pr^{1/2}$ (Schlichting & Gersten, 2000; Shishkina et al., 2017), while in regime I_u it holds $\lambda_u/\lambda_\theta \sim Pr^{1/3}$, all just as in the classical Prandtl-Blasius-Pohlhausen theory (Schlichting, 1979).

Equating ϵ_u (Equation 9) and ϵ_θ (Equation 10) to their estimated bulk or BL contributions, we obtain the scalings of $\tilde{\Delta}$ and Re in IHC, which are summarized in Table 1 and sketched in Figure 1.

Table 1
Scaling Relations for ϵ_u, ϵ_θ, $\tilde{\Delta}$, and Re in the Different Limiting Regimes in IHC

Regime	$\epsilon_u/(\nu^3 L^{-4})$ $\sim Pr^{-2}Rr$	ϵ_θ / $(\kappa\Delta^2 L^{-2})$ $\sim \tilde{\Delta}^{-1}$	$\tilde{\Delta}$	Re
$I_\infty^<$	$\sim Re^2$	$\sim Pr^{1/2}Re^{1/2}$	$\sim Pr^0\, Rr^{-1/4}$	$\sim Pr^{-1}\, Rr^{1/2}$
I_u	$\sim Re^{5/2}$	$\sim Pr^{1/3}Re^{1/2}$	$\sim Pr^{1/15}\, Rr^{-1/5}$	$\sim Pr^{-4/5}\, Rr^{2/5}$
I_ℓ	$\sim Re^{5/2}$	$\sim Pr^{1/2}Re^{1/2}$	$\sim Pr^{-1/10}\, Rr^{-1/5}$	$\sim Pr^{-4/5}\, Rr^{2/5}$
II_ℓ	$\sim Re^3$	$\sim Pr^{1/2}Re^{1/2}$	$\sim Pr^{-1/6}\, Rr^{-1/6}$	$\sim Pr^{-2/3}\, Rr^{1/3}$
III_∞	$\sim Re^2$	$\sim Pr\, Re\tilde{\Delta}$	$\sim Pr^0\, Rr^{-1/4}$	$\sim Pr^{-1}\, Rr^{1/2}$
IV_u	$\sim Re^3$	$\sim Pr\, Re^{3/2}\tilde{\Delta}$	$\sim Pr^0\, Rr^{-1/4}$	$\sim Pr^{-2/3}\, Rr^{1/3}$
IV_ℓ	$\sim Re^3$	$\sim Pr\, Re$	$\sim Pr^{-1/3}\, Rr^{-1/3}$	$\sim Pr^{-2/3}\, Rr^{1/3}$

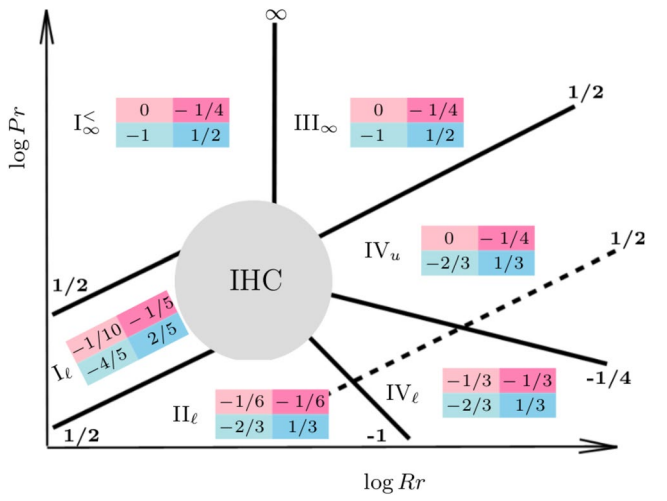

Figure 1. Sketch of the phase space of IHC with the various limiting scaling regimes following from our unifying theory. Continuous lines show the slopes of the transitions between the different regimes. The exponent β_0 of each slope $Pr \sim Rr^{\beta_0}$ between the different regimes in phase space is written in bold, close to the corresponding line. The dashed line shows the slope of the transition to the ultimate regime. For each regime, the color box represents the scaling exponents in the scalings of $\tilde{\Delta}$ and Re versus Pr and Rr: $\begin{cases} \tilde{\Delta} \sim Pr^{\beta_1} Rr^{\beta_2} \\ Re \sim Pr^{\beta_3} Rr^{\beta_4} \end{cases}$. This phase space for IHC is the analogous one to the one of RBC of Grossmann and Lohse (2001) and the one of HC in Shishkina et al. (2016). Our two-dimensional DNS cover Regime I_ℓ and $I_\infty^<$.

As already mentioned above, the very same idea was already applied to HC (Shishkina et al., 2016). Interestingly enough, even a formal analogy between IHC and HC exists, out of which we could have already derived the scaling relations of Table 1 and Figure 1. The reason for this formal analogy is that the relations obtained for ϵ_θ and ϵ_u (see Equations 5 and 6 of Shishkina et al. [2016]) formally resemble the corresponding relations 9 and 10 here. For the first equation this becomes particular obvious when writing $\epsilon_\theta = \frac{L^2}{\kappa}\Omega^2\tilde{\Delta} = \frac{\kappa}{L^2}\Delta^2\tilde{\Delta}^{-1}$ and for the second when realizing that $\left(\frac{1}{2} - \tilde{Q}_0\right)$ is only a dimensionless factor between 0 and 1/2. Then one sees immediately that the role of the control parameter Ra in HC is taken by that of the control parameter Rr in IHC and the role of the response parameter Nu in HC is taken by that of the (inverse) response parameter $\tilde{\Delta}^{-1}$ in IHC. All derived scaling relations in the different limiting regimes of HC can directly be taken over. The corresponding values for IHC give the same results as obtained above and have already been shown in Table 1 and Figure 1.

4. Comparison With Direct Numerical Simulations

To check these predictions of the GL theory generalized to IHC, we have performed 2-D DNS according to Equations 1 and 2 with the corresponding BCs. We chose an aspect ratio of $\Gamma = 2$ for the laterally periodic box. The numerics have been validated by making sure that the exact relations 9 and 10 are fulfilled. Simulations were performed using the second-order staggered finite difference code AFiD (van der Poel et al., 2015; Verzicco & Orlandi, 1996). This code has already been extensively used to study RBC (see Wang et al., 2020a, 2020b).

The parameter combinations (Rr, Pr) for which we performed simulations are shown in the parameter space of Figure 2a. A typical snapshot of the temperature field together with the mean temperature profile for one parameter combination are displayed in Figure 2b. One can see the stably stratified layer near the bottom plate. The interaction of the upper convection zone and the lower stably stratified region leads to the so-called penetrative convection (Veronis, 1963; Wang et al., 2019). The mean temperature profile, which, as expected and typical for IHC, displays top-down asymmetry.

The results for the response parameters $\tilde{\Delta}$ and Re as functions of the control parameters Rr and Pr are shown in Figures 3 and 4. As can be seen, in general, there are no pure scaling laws over the simulated range, but smooth crossovers from one regime to the other, very similarly as in RBC (Stevens et al., 2013), reflecting the key idea of the unifying theory by Grossmann and Lohse (2000, 2001). We first discuss the dependences for the dimensionless mean temperature $\tilde{\Delta}$, see Figures 3a and 3b. As a function of Pr (Figure 3b), for all Rr the transition from $\tilde{\Delta} \sim Pr^{-1/10}$ of regime I_l to the Pr-independence of regime $I_\infty^<$ can clearly be seen. The more turbulent regimes $IV_{u,\ell}$ are not yet realized, as the driving is not strong enough. This is also reflected in the Rr dependence $\tilde{\Delta} \sim Rr^{-1/5}$ reflecting that of regimes $I_{u,\ell}$. No indication to a stronger dependence as typical for the more turbulent regimes $IV_{u,\ell}$ can yet be seen. This is also seen in the dependences of the Reynolds number (Figures 3c and 3d): For small $Pr \leq 1$, it goes like $Re \sim Rr^{2/5}$ as in regimes $I_{u,\ell}$. For large $Pr = 10$ the results are consistent with $Re \sim Rr^{1/2}$ as in regime $I_\infty^<$. This scaling should go hand in hand with the scaling $\tilde{\Delta} \sim Rr^{-1/4}$ for the dimensionless mean

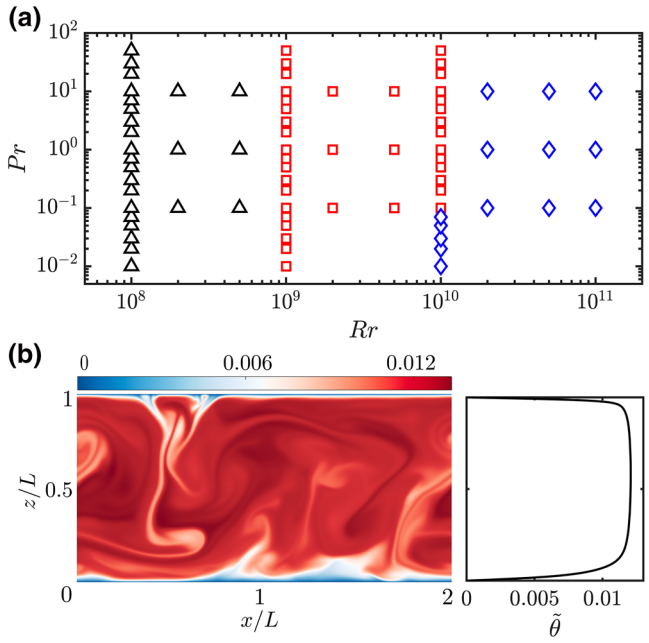

Figure 2. (a) Rr versus Pr parameter space of the simulated cases. Symbols denote the different grid resolutions used in DNS: 512×256 (△), 1024×512 (□), 2048×1024 (◇). (b) Instantaneous temperature field (color coded) and mean temperature profile for $Rr = 10^{10}$ and $Pr = 1$.

temperature, but as seen from Figure 3a, those data are presumably better described by $\tilde{\Delta} \sim Rr^{-1/5}$. Finally, on the Pr-dependence of Re: As seen from Figure 3d, for all Rr the data show a transition from the $Re \sim Pr^{-4/5}$ scaling of regimes $I_{u,\ell}$ to the $Re \sim Pr^{-1}$ scaling of regime $I^{<}_{\infty}$, consistent with the corresponding transition for $\tilde{\Delta}$ in Figure 3b.

All these results are consistent with our unifying theory, which however goes much beyond the simulated parameter range into the regimes in which the kinetic and thermal energy dissipation rates are dominated by the turbulent bulk contributions. These regimes are inaccessible with our present numerical simulations, even in 2-D.

As an additional check of our unifying theory we also plot the kinetic energy dissipation rate as function of Re, see Figure 5. Indeed, we find $\epsilon_u/(L^3\nu^{-4}) \sim Re^{5/2}$ and $\sim Re^2$ as characteristic for the kinetic BL dominated regimes $I_{u,\ell}$ and $I^{<}_{\infty}$, consistent with what we have seen in Table 1 and Figure 3.

Another (less important) response parameter of IHC is the magnitude of the dimensionless heat flux $\tilde{Q}_0$ through the bottom plate. The numerical results for $\tilde{Q}_0$ are shown in Figure 6. One sees from Figure 6a that $\tilde{Q}_0$ only weakly depends on Rr in the present parameter range; this behavior has also been found before in Goluskin and van der Poel (2016). Figure 6b illustrates that much less heat is transported outwards from the bottom plate with increasing Pr. The small $\tilde{Q}_0$ for large Pr is due to the less efficient shear-driven mixing of the fluid near the bottom plate.

5. Conclusions

In conclusion, in the spirit of the prior unifying theories for RBC (Grossmann & Lohse, 2000, 2001) and for HC (Shishkina et al., 2016), in this paper we have developed a unifying theory of IHC for the scaling of the mean temperature and the Reynolds number as functions of the control parameters Rr and Pr. The main

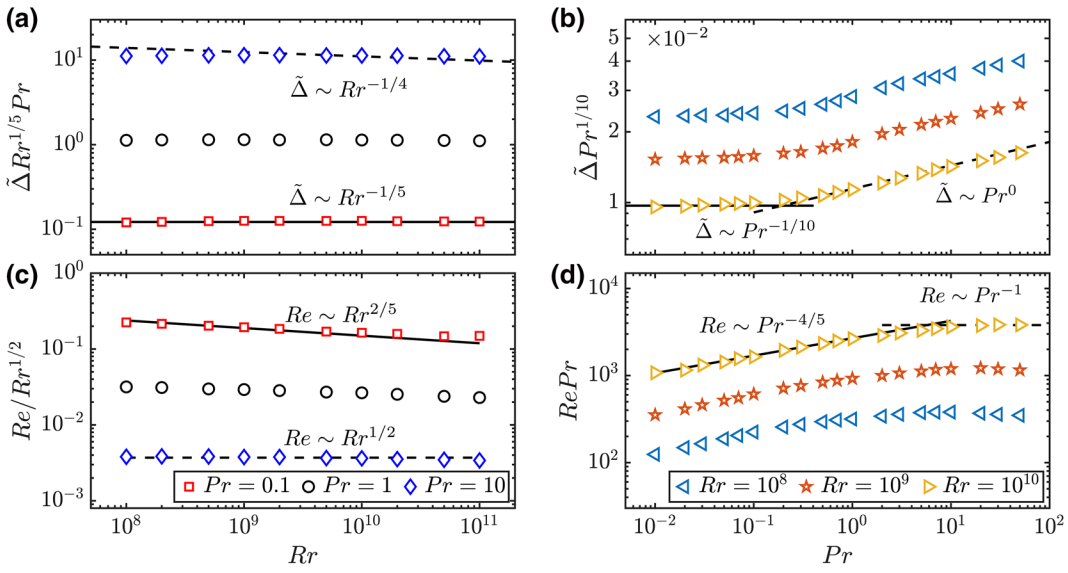

Figure 3. Response parameters $\tilde{\Delta}$ (the dimensionless mean temperature of the bulk) and Re as function of the control parameters Rr and Pr: (a) Compensated $\tilde{\Delta}$ as function of Rr for fixed $Pr = 10^{-1}$, 1, 10. (b) Compensated $\tilde{\Delta}$ as function of Pr for fixed $Rr = 10^8$, 10^9, 10^{10}. (c) Compensated Re as function of Rr for fixed $Pr = 10^{-1}$, 1, 10. (d) $RePr$ as function of Pr for fixed $Rr = 10^8$, 10^9, 10^{10}. The straight lines with the corresponding scaling laws are added as guide to the eye.

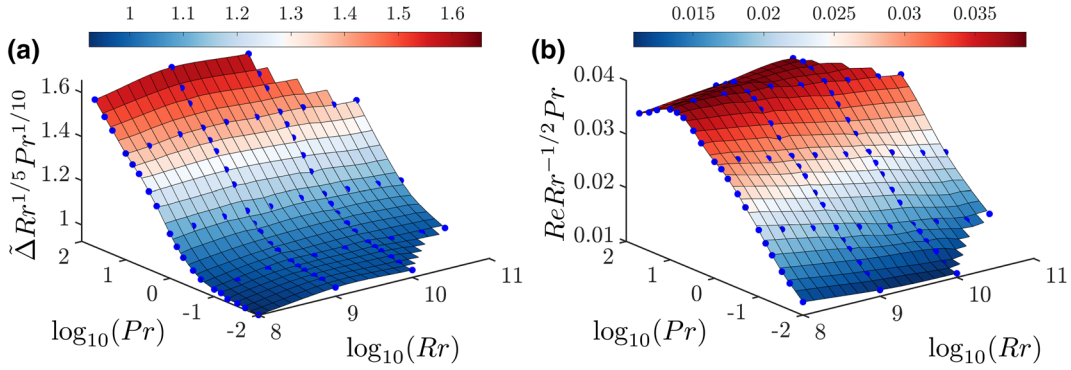

Figure 4. Compensated three-dimensional visualization of (a) $\tilde{\Delta}(Ra, Pr)$ and (b) $Re(Ra, Pr)$.

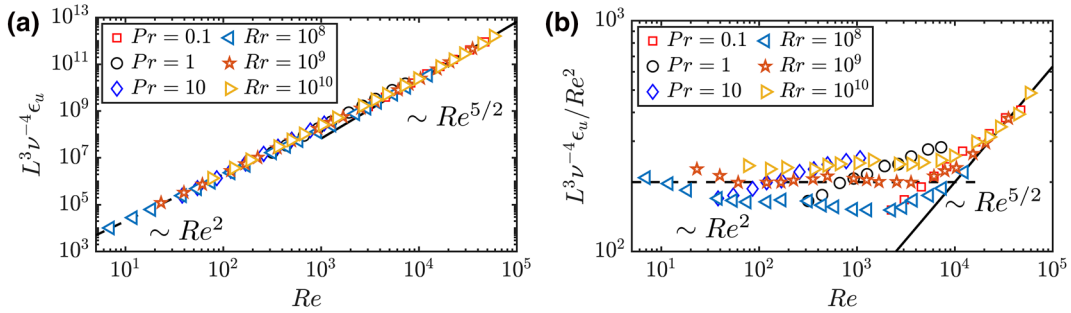

Figure 5. The nondimensionalized (a) absolute kinetic energy dissipation rate $L^3\nu^{-4}\epsilon_u$ and (b) compensated kinetic energy dissipation rate $L^3\nu^{-4}\epsilon_u/Re^2$ as functions of Re. Note that $L^3\nu^{-4}\epsilon_u \sim RrPr^{-2}$, Equation 10, holds exactly throughout and has numerically been checked for consistency (not shown). Also note that the nondimensionalized thermal energy dissipation rate (middle column of Table 1) is nothing else but $\sim \tilde{\Delta}^{-1}$ and has thus already been shown in Figures 3a and 3b.

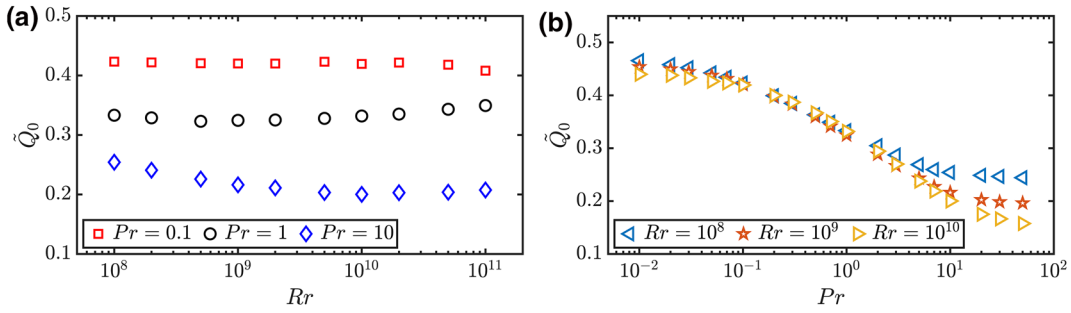

Figure 6. Magnitude of the dimensionless heat flux through the bottom plate, $\tilde{Q}_0$, as function of (a) Ra for the different Pr and (b) Pr for the different Ra (also shown in legends).

result is visualized in Figure 1. We have shown that the 2-D DNS results are consistent with this theory, though the numerically accessible regimes are still dominated by the BLs, and not all predictions of the theory can already be tested at this point. Also 3-D DNS over a large fraction of the control parameter space are presently too demanding from the viewpoint of computational cost and have not yet been done. We have furthermore pointed toward the formal analogy between IHC and HC and it will be illuminating to explore this analogy also numerically.

Data Availability Statement

The data used in this paper are available for download at http://doi.org/10.5281/zenodo.4081485.

Acknowledgments
R. Verzicco, D. Goluskin, and K. L. Chong are gratefully acknowledged for discussions and support. The authors also acknowledge the Twente Max-Planck Center, the Deutsche Forschungsgemeinschaft (Priority Programme SPP 1881 "Turbulent Superstructures"), PRACE for awarding us access to MareNostrum 4 based in Spain at the Barcelona Computing Center (BSC) under PRACE project 2020225335. The simulations were partly carried out on the national e-infrastructure of SURFsara, a subsidiary of SURF cooperation, the collaborative ICT organization for Dutch education and research. Q. Wang acknowledges financial support from China Scholarship Council (CSC) and Natural Science Foundation of China under grant no. 11621202.

References

Ahlers, G., Grossmann, S., & Lohse, D. (2009). Heat transfer and large scale dynamics in turbulent Rayleigh-Bénard convection. *Reviews of Modern Physics*, *81*, 503–537.

Bercovici, D., Schubert, G., & Glatzmaier, G. A. (1989). Three-dimensional spherical models of convection in the Earth's mantle. *Science*, *244*(4907), 950–955.

Bunge, H.-P., Richards, M. A., & Baumgardner, J. R. (1996). Effect of depth-dependent viscosity on the planform of mantle convection. *Nature*, *379*(6564), 436–438.

Chilla, F., & Schumacher, J. (2012). New perspectives in turbulent Rayleigh-Bénard convection. *The European Physical Journal. E, Soft Matter*, *35*, 58.

Ching, E. S. C., Leung, H. S., Zwirner, L., & Shishkina, O. (2019). Velocity and thermal boundary layer equations for turbulent Rayleigh-Bénard convection. *Physical Review Research*, *1*, 033–037.

Goluskin, D. (2016). *Internally heated convection and Rayleigh-Bénard convection*. Springer.

Goluskin, D., & Spiegel, E. A. (2012). Convection driven by internal heating. *Physics Letters A*, *377*(1–2), 83–92.

Goluskin, D., & van der Poel, E. P. (2016). Penetrative internally heated convection in two and three dimensions. *Journal of Fluid Mechanics*, *791*, R6.

Grossmann, S., & Lohse, D. (2000). Scaling in thermal convection: A unifying view. *Journal of Fluid Mechanics*, *407*, 27–56.

Grossmann, S., & Lohse, D. (2001). Thermal convection for large Prandtl number. *Physical Review Letters*, *86*, 3316–3319.

Grossmann, S., & Lohse, D. (2002). Prandtl and Rayleigh number dependence of the Reynolds number in turbulent thermal convection. *Physical Review E*, *66*, 016305.

Grossmann, S., & Lohse, D. (2004). Fluctuations in turbulent Rayleigh-Bénard convection: The role of plumes. *Physics of Fluids*, *16*, 4462–4472.

Houseman, G. (1988). The dependence of convection planform on mode of heating. *Nature*, *332*(6162), 346–349.

Hughes, G. O., & Griffiths, R. W. (2008). Horizontal convection. *Annual Review of Fluid Mechanics*, *40*, 185–208.

Kim, H., Boysen, D. A., Newhouse, J. M., Spatocco, B. L., Chung, B., Burke, P. J., et al. (2013). Liquid metal batteries: Past, present, and future. *Chemical Reviews*, *113*(3), 2075–2099.

Lay, T., Hernlund, J., & Buffett, B. A. (2008). Core–mantle boundary heat flow. *Nature Geoscience*, *1*(1), 25.

Lohse, D., & Xia, K.-Q. (2010). Small-scale properties of turbulent Rayleigh-Bénard convection. *Annual Review of Fluid Mechanics*, *42*, 335–364.

Mallard, C., Coltice, N., Seton, M., Müller, R. D., & Tackley, P. J. (2016). Subduction controls the distribution and fragmentation of earth's tectonic plates. *Nature*, *535*(7610), 140–143.

McKinnon, W. B., Nimmo, F., Wong, T., Schenk, P. M., White, O. L., Roberts, J. H., et al. (2016). Convection in a volatile nitrogen-ice-rich layer drives Pluto's geological vigour. *Nature*, *534*(7605), 82–85.

Moore, W. B., & Webb, A. A. G. (2013). Heat-pipe earth. *Nature*, *501*(7468), 501–505.

Ng, C. S., Ooi, A., Lohse, D., & Chung, D. (2015). Vertical natural convection: Application of the unifying theory of thermal convection. *Journal of Fluid Mechanics*, *764*, 349–361.

Ng, C. S., Ooi, A., Lohse, D., & Chung, D. (2017). Changes in the boundary-layer structure at the edge of the ultimate regime in vertical natural convection. *Journal of Fluid Mechanics*, *825*, 550–572.

Ng, C. S., Ooi, A., Lohse, D., & Chung, D. (2018). Bulk scaling in wall-bounded and homogeneous vertical natural convection. *Journal of Fluid Mechanics*, *841*, 825–850.

Roberts, P. H. (1967). Convection in horizontal layers with internal heat generation. *Journal of Fluid Mechanics*, *30*(1), 33–49.

Schlichting, H. (1979). *Boundary layer theory* (7th ed.). New York, NY: McGraw Hill.

Schlichting, H., & Gersten, K. (2000). *Boundary layer theory* (8th ed.). Berlin: Springer Verlag.

Schubert, G., Turcotte, D. L., & Olson, P. (2001). *Mantle convection in the Earth and planets*. Cambridge University Press.

Shishkina, O. (2016). Momentum and heat transport scalings in laminar vertical convection. *Physical Review E*, *93*, 051102(R).

Shishkina, O., Emran, M., Grossmann, S., & Lohse, D. (2017). Scaling relations in large-Prandtl-number natural thermal convection. *Physical Review Fluids*, *2*(103), 502.

Shishkina, O., Grossmann, S., & Lohse, D. (2016). Heat and momentum transport scalings in horizontal convection. *Geophysical Research Letters*, *43*, 1219–1225. https://doi.org/10.1002/2015GL067003

Shishkina, O., & Horn, S. (2016). Thermal convection in inclined cylindrical containers. *Journal of Fluid Mechanics*, *790*, R3.

Shishkina, O., Horn, S., Wagner, S., & Ching, E. S. C. (2015). Thermal boundary layer equation for turbulent Rayleigh–Bénard convection. *Physical Review Letters*, *114* 114302.

Shishkina, O., & Wagner, S. (2016). Prandtl-number dependence of heat transport in laminar horizontal convection. *Physical Review Letters*, *116* 024302.

Shraiman, B. I., & Siggia, E. D. (1990). Heat transport in high-Rayleigh number convection. *Physical Review A*, *42*, 3650–3653.

Stevens, R. J. A. M., Blass, A., Zhu, X.-J., Verzicco, R., & Lohse, D. (2018). Turbulent thermal superstructures in Rayleigh-Bénard convection. *Physical Review Fluids*, *3*(4), 041501.

Stevens, R. J. A. M., van der Poel, E. P., Grossmann, S., & Lohse, D. (2013). The unifying theory of scaling in thermal convection: The updated prefactors. *Journal of Fluid Mechanics*, *730*, 295–308.

Tackley, P. J., Stevenson, D. J., Glatzmaier, G. A., & Schubert, G. (1993). Effects of an endothermic phase transition at 670 km depth in a spherical model of convection in the Earth's mantle. *Nature*, *361*(6414), 699–704.

Tritton, D. J. (1975). Internally heated convection in the atmosphere of Venus and in the laboratory. *Nature*, *257*(5522), 110–112.

Tritton, D. J., & Zarraga, M. N. (1967). Convection in horizontal layers with internal heat generation. *Journal of Fluid Mechanics*, *30*(1), 21–31.

Trowbridge, A. J., Melosh, H. J., Steckloff, J. K., & Freed, A. M. (2016). Vigorous convection as the explanation for Pluto's polygonal terrain. *Nature*, *534*(7605), 79–81.

van der Poel, E. P., Ostilla-Mónico, R., Donners, J., & Verzicco, R. (2015). A pencil distributed finite difference code for strongly turbulent wall-bounded flows. *Computers & Fluids*, *116*, 10–16.

van der Poel, E. P., Stevens, R. J. A. M., & Lohse, D. (2013). Comparison between two- and three-dimensional Rayleigh-Bénard convection. *Journal of Fluid Mechanics*, *736*, 177–194.

Veronis, G. (1963). Penetrative convection. *The Astrophysical Journal*, *137*, 641.

Verzicco, R., & Orlandi, P. (1996). A finite-difference scheme for three-dimensional incompressible flows in cylindrical coordinates. *Journal of Computational Physics*, *123*(2), 402–414.

Vilella, K., & Deschamps, F. (2017). Thermal convection as a possible mechanism for the origin of polygonal structures on Pluto's surface. *Journal of Geophysical Research: Planets*, *122*(5), 1056–1076. https://doi.org/10.1002/2016JE005215

Vilella, K., Limare, A., Jaupart, C., Farnetani, C. G., Fourel, L., & Kaminski, E. (2018). Fundamentals of laminar free convection in internally heated fluids at values of the Rayleigh–Roberts number up to 10^9. *Journal of Fluid Mechanics*, *846*, 966–998.

Wang, Q., Chong, K.-L., Stevens, R. J. A. M., Verzicco, R., & Lohse, D. (2020b). From zonal flow to convection rolls in Rayleigh-Bénard convection with free-slip plates. *Journal of Fluid Mechanics*, *905*, A21.

Wang, Q., Verzicco, R., Lohse, D., & Shishkina, O. (2020a). Multiple states in turbulent large-aspect ratio thermal convection: What determines the number of convection rolls? *Physical Review Letters*, *125*(074), 501.

Wang, Q., Zhou, Q., Wan, Z.-H., & Sun, D.-J. (2019). Penetrative turbulent Rayleigh–Bénard convection in two and three dimensions. *Journal of Fluid Mechanics*, *870*, 718–734.

Xiang, L., & Zikanov, O. (2017). Subcritical convection in an internally heated layer. *Physical Review Fluids*, *2*(6), 063501.

Yang, R., Chong, K. L., Wang, Q., Verzicco, R., Shishkina, O., & Lohse, D. (2020). Periodically modulated thermal convection. *Physical Review Letters*, *125*, 154502.

Yang, Y., Verzicco, R., & Lohse, D. (2018). Two-scalar turbulent Rayleigh-Bénard convection: Numerical simulations and unifying theory. *Journal of Fluid Mechanics*, *848*, 648–659.